Geosystems and Geoenvironment 2 (2023) 100133

Contents lists available at ScienceDirect

Geosystems and Geoenvironment

journal homepage: www.elsevier.com/locate/geogeo

Clay mineralogy and provenance modeling of the Paleoproterozoic Kaladgi shales, Dharwar Craton, Southern India: Implications on paleoweathering and source rock compositions

Pronoy Roy[a,b], G. Parthasarathy[c], Bulusu Sreenivas[a,b,*]

[a] CSIR-National Geophysical Research Institute, Hyderabad 500007, India
[b] Academy of Scientific and Innovative Research (AcSIR), Ghaziabad 201002, India
[c] School of Natural Sciences and Engineering, National Institute of Advanced Studies, Bangalore 560012, India

ARTICLE INFO

Article history:
Received 11 May 2022
Revised 23 August 2022
Accepted 13 September 2022

Handling Editor: Sohini Ganguly

Keywords:
Paleoproterozoic
Kaladgi Supergroup
Shales
XRD analysis
Provenance
Geochemical modelling

ABSTRACT

Proterozoic clastic sediments reveal vast information regarding provenance, depositional conditions, and environmental evolutions. Peninsular India comprising Archean cratons, also have numerous intracratonic Proterozoic sedimentary basins along their margins. The Archean Dharwar Craton in southern India has many Proterozoic successions, namely Cuddapah, Kurnool towards the East, and Kaladgi, Badami, and Bhima towards the northern margin. The Paleoproterozoic Kaladgi Basin (~1.85 Ga) consists of siliciclastic sedimentary rocks with stromatolitic carbonate formations. XRD analysis of shale layers of the Lower Lokapur and Upper Simikere subgroups have been carried out to understand the primary clay mineral assemblages, weathering history, and provenance. The Lower and Upper shale layers of Lokapur and Simikere subgroups show a dominance of montmorillonite and kaolinite, respectively. The geochemical affinities and the clay mineral assemblages indicate a more mafic source to the lower shales (Manoli and Hebbal formations) and increased felsic contribution to the upper shales (Govindakoppa and Daddanhatti formations). Illite is ubiquitous in all the shales of the Kaladgi Supergroup possibly representing the diagenetic transformation of montmorillonite and kaolinite to illite. Geochemical modeling of provenance has been carried out using $(Eu/Eu^*)_N$, $(La/Yb)_N$, $(Gd/Yb)_N$, and $(La/Sm)_N$ of all the plausible source rocks and the average compositions of lower and upper shales. The modeling results suggest that the lower shales are derived from a source of mafic rocks – 45 %, K-rich granite – 35 %, and TTG – 20 %. While the upper shales are derived from source characterized by K-rich granites – 61 % and intermediate volcanic rocks – 39 %. These results signify the classical unroofing of TTG-greenstone belts exposing K-rich granites with the progression of sedimentation. Further, a good correlation between K-enrichment (a measure of % difference between CIA and pre-metasomatic CIA) and ΣLREE is attributed to the abundance of kaolinites that fractionate more LREE.

1. Introduction

Earth's middle age ranging from ~1.8 to 1.0 Ga, is referred to as the "Boring Billion", the "Dullest time", the "Barren Billion" is known for its geochemical stasis and glacial stagnation (Buick et al., 1995; Brasier, 2012; Young, 2013). The relatively flat carbon isotope record (Gilleaudeau and Kah, 2013), low atmospheric oxygen levels (Holland, 2006), tectonic quiescence (Roberts, 2013; Cawood and Hawkesworth, 2014), no known glaciations (Young, 1988), and delayed organic evolution (Planavsky et al., 2014) – all characterize Earth's middle age. The preceding (Paleoproterozoic) and following (Neoproterozoic periods of these middle ages have witnessed dramatic shifts in atmospheric oxygen levels known as the Great Oxidation Event (GOE; Lyons et al., 2014), glaciations (Young, 1988), and carbon isotope excursions (Karhu and Holland, 1996; Knoll et al., 1986). Understanding the Earth's middle age is one of the critical questions.

The Proterozoic mobile belts and epicratonic platform basins (Purana basins) encompassing the Archean cratonic nuclei represent the Proterozoic history of Peninsular India (Radhakrishna and Naqvi, 1986; Kale and Phansalkar, 1991; Vaidyanathan and Ramakrishnan, 2010; Mazumdar and Eriksson, 2015). The Purana

* Corresponding author.
E-mail address: bsreenivas@ngri.res.in (B. Sreenivas).

https://doi.org/10.1016/j.geogeo.2022.100133

basins are dominated mainly by deposition of thick sequences of clastic/non-clastic shallow marine sediments (Eriksson et al., 1998; Kale et al., 2016). The ages range between Late Paleoproterozoic (1.9 Ga) and Neoproterozoic, constituting India's most widespread Pre-Gondwana deposits (Collins et al., 2015; Joy et al., 2019). The Purana basins correlate temporally with supercontinents Colombia, Rodinia, and Gondwana (Basu and Bickford, 2015; Saha et al., 2016; Absar et al., 2016). The Cuddapah-Kurnool, Pranhita-Godavari, Kaladgi-Badami, and Bhima basins are the Proterozoic basins in the southern part of India on the peripheries of the Archean Dharwar Craton.

The Proterozoic Kaladgi-Badami Basin lies in the Northern part of the Western Dharwar Craton (WDC). It constitutes sedimentary archives that can provide vital information on the provenance and paleoenvironment prevalent during the Late Paleo- and Mesoproterozoic history of the Earth. The sediments of the Kaladgi-Badami Basin cover a period from ~1.8 to 0.8 Ga, the "Boring billion" years. The shales are fine-grained siliciclastics consisting of clay minerals and are considered excellent proxies to infer provenance and paleoenvironment history (McCulloch and Wasserburg, 1978; Yang et al., 2019). However, diagenetic and metamorphic effects must be examined and appropriately assessed as shales are prone to secondary alterations (Nesbitt and Young, 1989; Zhang et al., 1998; Cullers and Podkovyrov, 2000; Mishra and Sen, 2012).

The X-Ray Diffraction (XRD) and Differential Thermal Analysis (DTA) studies on shales provide critical evidence that helps reconstruct the weathering conditions affecting the parent rocks, Eh-Ph ratio, water-rock ratios, and salinity of the depositional environment. The different parameters calculated from XRD studies like illite crystallinity index (IC), lattice parameter indicating phengite content (b_o values; barometric indicators), and kaolinite/illite ratios provide crucial information related to the clay mineral assemblages, thermal maturity, pressure, temperature, and fluid activity attested by the shales during diagenesis (Velde, 1995). Previous studies on the shales of the Kaladgi Basin by (Rao et al., 1999) focused on the geochemistry of the shales. They inferred the provenance of the sediments in the Kaladgi Basin consisted of mafic to felsic rocks in the ratio of 60:40. The high potassic content in Kaladgi shales and LREE enrichment was suggested due to post-depositional metasomatism (Rao et al., 1999). Dey et al. (2008a, 2008b) refuted the idea of K-enrichment in shales due to metasomatism based on presence of detrital K feldspar in shales and paleoweathered basement indicating substantial involvement of potassic-rich granites in the provenance. Mukherjee et al. (2016, 2019) identified different clay minerals and studied the metamorphic grade and thermal maturity using the IC values. Based on variations observed in the IC values along and across the basin, they proposed southerly directed gravity gliding deformation.

This study presents XRD analysis of Kaladgi shales and attempts provenance modeling to constrain crustal sources and effects of K-metasomatism. The provenance modeling method adopted in this study is after Kasanzu et al. (2008), which involves the use of critical REE ratios, including $(Eu/Eu^*)_N$, $(La/Yb)_N$, $(Gd/Yb)_N$, $(La/Sm)_N$ of all the plausible source rocks surrounding the basin. The compositions of shales are arranged in the form of a matrix equation to characterize and estimate the percentage contribution of all the possible source rocks.

2. Geological setting

The Kaladgi-Badami Basin lies in the northern part of the Western Dharwar Craton (WDC) and occupies about 8000 km^2 (Fig. 1). The thickness of the sedimentary succession is around 3900 m (Dey, 2015; Jayaprakash et al., 1987). The Late Cretaceous Deccan traps mostly bound the Northern and Western parts of the basin. While some parts of the Kaladgi Basin lie underneath these traps, some occur as inliers within the Deccan traps (Raha and Sastry, 1982). The Late Archean Hungund-Kushtagi greenstone belts, TTGs of Western Dharwar Craton, and metasediments of Dharwar Supergroup are the basement rocks of this basin. The Kaladgi Basin is mainly dominated by siliciclastics and platform carbonate sediments overlying the Archean basement. The lithostratigraphic classification of the Kaladgi Supergroup is shown in Table 1. The Kaladgi Supergroup (KSG) is subdivided into the Bagalkot and Badami groups . Geochemical compositions of argillites of the Manoli, Hebbal members of the Lower Lokapur Subgroup (LSG) and the Govindakoppa, Daddanhatti argillites of the Upper Simikeri Subgroup (SSG; from Rao et al., 1999) have been used in this study for modeling the provenance. The deformed rock formations have been metamorphosed to sub-greenschist facies conditions. Only a few radiometric ages have been reported from the Kaladgi Supergroup due to the paucity of igneous activity in the basin (Joy et al., 2019; Pillai et al., 2018; Kale and Phansalkar, 1991). The biostratigraphic correlation based on stromatolite morphology in the carbonate rocks suggests Riphean age (Jayaprakash et al., 1987). Based on the Rb-Sr model age, the depositional age of the shales from the Bagalkot group is suggested to be younger than 1800 ± 100 Ma (Padmakumari et al., 1998; Rao et al., 1999). Recently, dykes intruding the lower formations yielded a U-Pb baddeleyite age of 1861 ± 4 Ma (Joy et al., 2019), assigning the Orosirian age to the Lower Kaladgi Supergroup. Mafic dykes intruding in the Uppermost Hoskatti formation of the Simikeri Group yield a whole rock age of $^{40}Ar/^{39}Ar$ as 1154 ± 4 Ma (Pillai et al., 2018), suggesting that the termination of the Kaladgi Basin be Meso-Neoproterozoic age. The Kaladgi Supergroup has been correlated with ~1800 Ma old Cuddapah Supergroup in the southern Indian peninsula (Bhaskar Rao et al., 1995; Zachariah et al., 1999). The overlying Badami Group is assigned a Neoproterozoic age (Pillai et al., 2018), separated by disconformity from Kaladgi Supergroup, and mostly correlates with Bhima and Kurnool basins (Saha et al., 2016).

3. Sampling and analytical methods

3.1. Sampling

The shale samples were collected from four formations of the Kaladgi Supergroup viz. Ramdurg, Yendigeri (Lokapur Subgroup; Manoli; n = 5; and Hebbal; n = 2), Kundargi, Hoskatti (Simikere Subgroup; Govindakoppa; n = 7; and Daddanhatti; n = 2) mainly from the type areas, and have been analyzed in this study (Fig. 1). The brown to purple-colored Manoli argillites from the Ramdurg Formation show well-developed fissility. They are interbedded with quartzites. The Hebbal argillites of the Yendigeri Formation are soft, flaky, and smoky blue. These argillites are interbedded with Chikshellikeri limestones and Chitrabhanukot dolomites. The Govindakoppa argillites are mostly variegated shales having cyclic purple and brick red colored layers belonging to the Kundargi Formation and lie on top of Muchkundi quartzites. Daddanhatti shales are smoky blue and locally phyllitic belonging to the Hoskatti Formation and are overlain by mafic intrusives. The collected samples represent stratigraphically older to younger sequences in the Kaladgi Supergroup.

3.2. XRD analysis

Representative samples collected from the type area for the four Members have been split into clay and non-clay fractions following standard procedure (after Krumn and Buggisch, 1991; Warr and Rice, 1994). The disaggregated material is separated into ≥0.2 μm size fractions by dispersing them in water, and the clay fraction was separated from aqueous suspensions by centrifuging at 4000 rpm for 15 minutes. From the clay fractions, oriented slides with

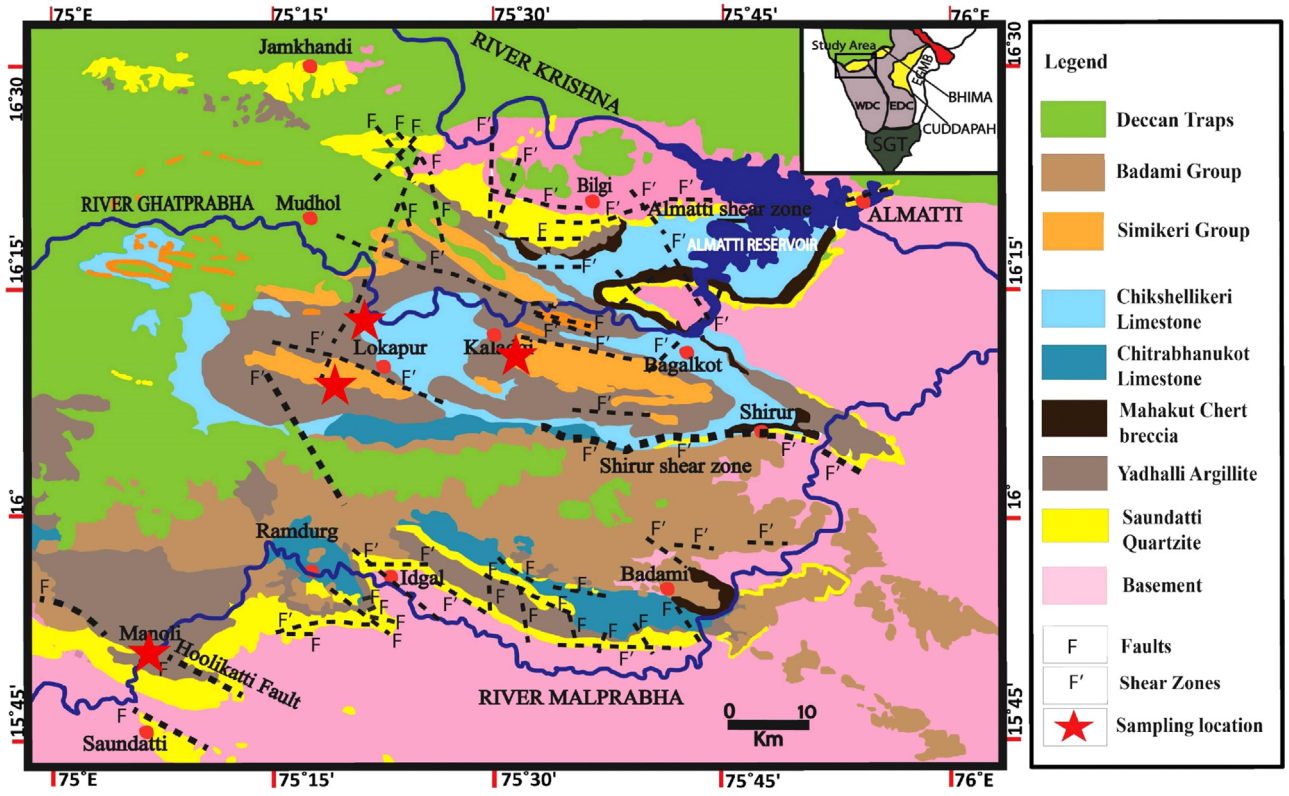

Fig. 1. Geological map of the Kaladgi Basin indicating locations of type areas from which shale/argillite samples have been collected (modified after Jayaprakash et al., 1987).

Table 1
Lithostratigraphy of the Kaladgi Supergroup (after Jayaprakash et al., 1987).

Era	Group	Subgroup	Formation	Member	Thickness (m)
Proterozoic	BADAMI		Katageri	Konkankoppa Limestone	85
				Halkurki Shale	67
			Kerur	Belikhindi Arenite	39
				Halgeri Shale	3
				Cave Temple Arenite	89
				Kendur Conglomerate	3
			——Angular unconformity————		
	BAGALKOT	SIMIKERI	Hoskatti	Mallapur Intursive	7
				Daddanhatti Argillite	695
			Arilkatti	Lakshnahatti Dolomite	87
				Kerkalmati Hematite schist	42
				Niralkeri Chert-Breccia	39
			Kundargi	**Govindakoppa Argillite**	80
				Muchkundi Quartzite	182
				Bevanmatti Conglomerate	15
			————————Disconformity————————		
	GROUP	LOKAPUR	Yadhalli	Argillite	58
			Muddapur	Bamanbudni Dolomite	402
				Petlur Limestone	121
				Jalikatti Argillite	43
			Yendigeri	Naganur Dolomite	93
				Chikshellikeri Limestone	883
				Hebbal Argillite	166
			Yargatti	Chitrabhankot Dolomite	218
				Muttalgeri Argillite	502
				Mahakut Chert-Breccia	133
			Ramdurg	**Manoli Argillite**	61
				Saundatti Quartzite	383
			——Nonconformity————		
Archaean			Granitoids, gneisses and metasediments of Dharwar Supergroup		

~3 mg clay layer /cm^2 have been prepared by air-drying aqueous suspensions (Kisch, 1991). These oriented clay slides were used to determine clay mineralogy and crystallinity. The oriented samples were treated with ethylene glycol vapors for 24 hours. Separable diffractograms were obtained for each glycolated sample to distinguish between montmorillonite and chlorite using the 14 Å peak. Oriented slides were also heated up to 550°C in an electric furnace to identify kaolinite. Kaolinite reflection maxima in the regions 001 and 002 were differentiated from those of chlorite by the absence of 001 and 003 reflections and the acid dissolution test (Brown, 1961).

The illite crystallinity index (IC) was calculated according to Kisch (1991). IC is determined by measuring the half-peak width of the 10 Å illite on oriented mineral aggregate preparations of the <2 μm size fractions and is expressed in $^\circ\Delta 2\theta$. To calibrate our IC data to Kisch's (1991), we measured the IC of well-crystallized pegmatitic muscovite (mica from the Rajasthan mica belt and Nellore mica belt, Andhra Pradesh) under identical XRD settings. Our estimated IC value for the well-crystallized mica is 0.084 $^\circ 2\theta$, which corresponds well with the value given by Kisch (1991). Powder X-ray diffraction studies (XRD) were carried out on bulk, ethylene glycolated, and heated samples using a D-5000 Siemens X-ray diffractometer at CSIR-IICT, Hyderabad. Cu Kα radiations (λ-1.5406 Å) were used throughout the measurements, along with a Ni filter and HOPG graphite monochromator. Two slits at the source side with a solid angle of 3° (Convergent side) and two slits with a solid angle of 0.03° and 0° on the detector side were used. Bulk shale samples were scanned in the (2θ = 5° to 60°), and all oriented clay slides were scanned through a range (2θ = 5° to 15°) under identical x-ray diffraction settings using quartz as the internal standard. The procedure of identifying and confirming different clay and non-clay minerals followed is after (Bailey, 1988). Most powdered XRD patterns exhibited peaks overlapping with more than two end members. The individual mineral phases were indexed with the help of https://rruff.info/RRUFF Sample Data compilation.

3.3. Differential thermal analysis (DTA)

The mineral compositions has been verified in a few representative samples by differential thermal analysis (DTA). The DTAhas been carried out at ambient pressure using Leeds and Northrop Thermal Analyzer, at a heating rate of 10 K/min at CSIR-IICT. The temperatures of the sample and the sample holder were measured with a Pt/Pt – 10 % Rh thermocouple. Typical uncertainty in the temperature measurements is 5 K at 1300 K. Samples of 250 mesh with weights varying between 20 and 40 mg were analyzed. A blank run was made to obtain the background signal. The instrument was calibrated with a well-known alpha-beta transition in quartz. Identifying various clay mineral phases was done by comparing our data with those of pure phases as listed by Smykatz-Kloss (1974).

4. Results

Powder X-ray diffraction patterns for raw, glycolated, and heated samples representing each of the four shale Members are given in Fig. 2, and corresponding mineral assemblages are listed in Table 2. Minerals identified by DTA are given in Table 3. The clay minerals present in the shales of the Kaladgi Supergroup are illite (Ilt), montmorillonite (Mnt), chlorite (Chl), kaolinite (Kln), and mixed-layer minerals (Mnt-Ilt and Mnt-Chl). The non-clay minerals present in the shales are quartz, trace amounts of carbonates, plagioclase feldspar, fluorapatite, pyroxene, and haematite. The XRD patterns of the clay minerals mostly show that they are ordered and crystallized, exhibiting prominent basal (001), (002), and (003) reflections (Fig. 2). Illite is the most common clay mineral present in all the shale samples of the Bagalkot Group.

The Lokapur and Simikeri subgroups of samples show similar mineral assemblages, but the proportions of individual mineral contents vary between them. Two samples from the Hebbal Member (P-6 and P-8) differ in their mineral composition from the lower Manoli Member, showing an assemblage of Ilt + Mnt + Chl and an absence of Kln. Most Manoli shales show a typical assemblage of Ilt + Mnt + Kln in decreasing order of abundance and mixed layer clays such as Ilt + Chl and Mnt + Chl in trace amounts. The frequency distribution of clay mineral assemblage points that lower members of the Kaladgi Supergroup are mainly dominated by Ilt and Mnt, except in sample T-6, where the assemblage Ilt + Mnt + Kln is dominant along with chlorite, as compared to clay mineral assemblage of upper shale members. The clay mineral assemblages belonging to the Simikeri Subgroup are Kln + Mnt + Chl + Ilt. About 30% of the samples contain only the Kln+Ilt mixed layer clays. However, one sample (D-2) of Daddanhatti members shows a mineral assemblage Mnt + Kln + Ilt + Chl in decreasing abundance. Mixed layer clays such as montmorillonite-chlorite are rarely detected in these samples, apart from only one sample (S-14) of the Govindakoppa member of the Simikeri Subgroup. The mineral kaolinite is the second most dominant in three samples and occurs in minor amounts in the rest of the samples.

The presence of chlorite would influence the XRD peak height of the kaolinite, because of which K and I cannot be estimated in chlorite-bearing samples. Samples were chosen accordingly to ensure proper estimation of the K/I value from powdered XRD peak heights (see Shrivastava and Ahmad, 2005). The average K/I value in the chlorite-free Govindakoppa shales (G2, G8, and G5) is 0.33, while this ratio is 0.26 for the Manoli shales (T6, T8, and T10). The K/I values suggest that Manoli Argillites, the lowermost shale, is characterized by a higher abundance of illite than the Govindakoppa Argillite of the Upper Simikeri Subgroup. Illite crystallinity (IC) has been extensively used to indicate the intensity of low-grade metamorphism (Weaver, 1989; Robinson et al., 1990; Yang and Hesse, 1991; Jha et al., 2012). The IC measures peak width at half the basal (001) reflection height. The IC distribution (Table 2; Fig. 3) indicates no apparent variations between Simikeri Subgroup and Lokapur Subgroup shales. Upper Simikeri Subgroup shales illite crystallinity ($^\circ\Delta 2\theta$) values range between (0.14°-0.30°), having a mean value around 0.21°. Similarly, Lower Lokapur Subgroup shales range from 0.20° to 0.25° with a mean of 0.21°. According to the classification of illite crystallinity (after Hesse and Dalton, 1991), the mean IC value of 2θ = 0.21° for the clays of the Bagalkot Group falls within the epi-metamorphic zone corresponding to the temperature of approximately 350°C. The approximate pressure range of the metamorphism is calculated with the help of b_o values from the $d_{(060)}$ peak position of illite. The values of illite (both of upper shale belonging to the Simikeri Subgroup and lower shales belonging to the Lokapur Subgroup) range from 8.87 Å to 9.036 Å with a mean value of 8.953 ± 006 Å. The average b_o value indicates that dioctahedral species (illite) is dominant and suggests that these sediments were subjected to low-pressure conditions. The (002)/(001) peak height ratio of illite, believed to be related to Al/(Al + Mg) ratios, reflects variations in metamorphic grade. The (002)/(001) average ratios of upper shales and lower shales are almost similar (Simikeri Subgroup = 0.35 ± 0.08; Lokapur Subgroup = 0.36 ± 0.07) and are compatible with uniform illite crystallinity values.

The results of the DTA on the Kaladgi shales are listed in Table 3. The clay minerals assemblages found by the DTA method validate the results of powder X-ray diffraction studies. DTA results confirm that in some samples of the lower Lokapur Subgrup shales (T-11 and T-6), chlorite is present in traces, while chlorite is absent

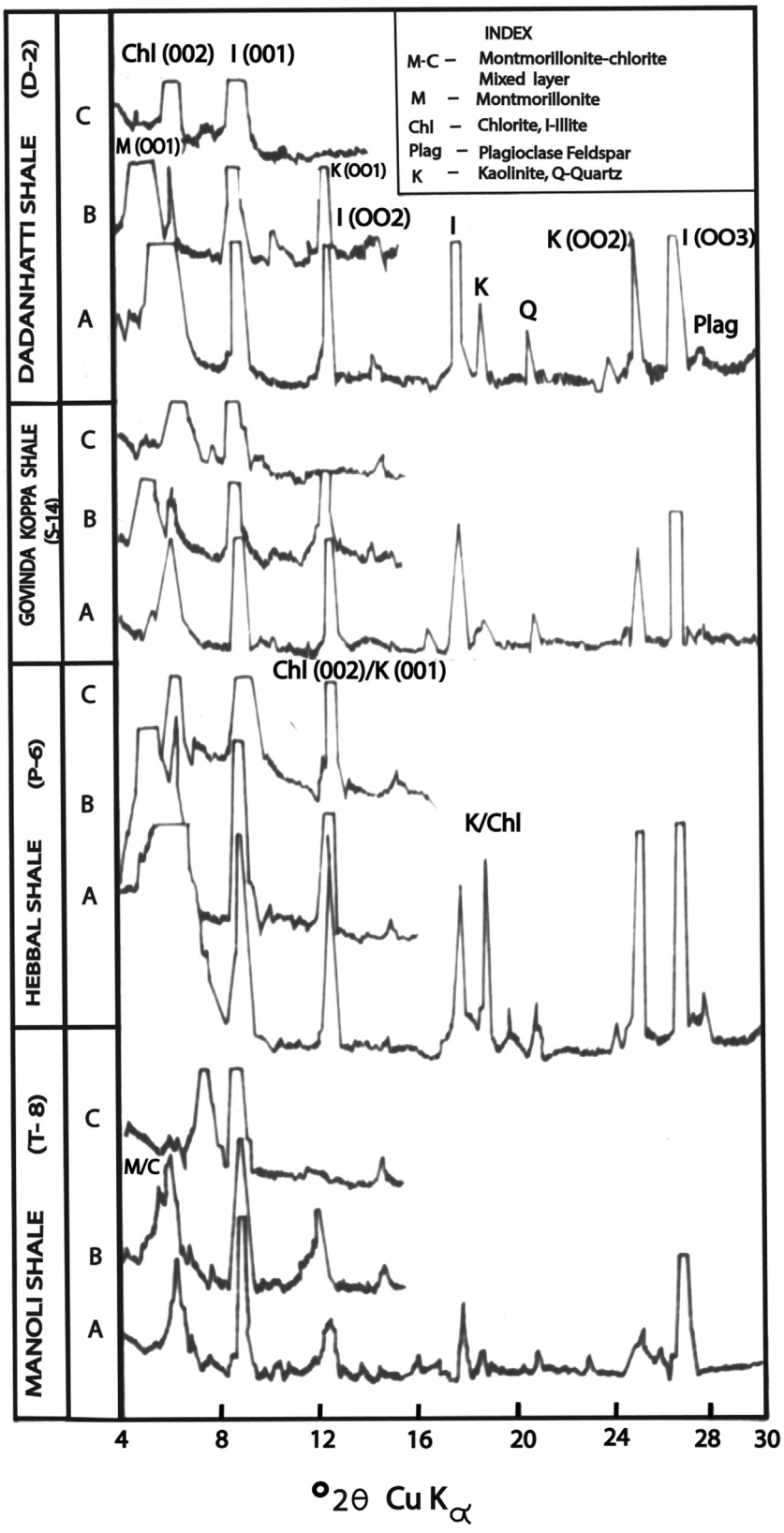

Fig. 2. XRD patterns of lower and upper Kaladgi shales.

Table 2
Powder X-ray diffraction data on clay minerals of shales of the Bagalkot Group.

Sample No.	Mineral assemblage Major	Minor	Trace	Illite characterstics IC	K/I	(002/001)	bo
Simikeri Subgroup							
D-2	Mnt+Ilt+Kln	Chl+Qz	Fap, Pl	0.20	0.54	0.45	8.870
S-17	Ilt+Kln	Mnt+Qz	Hem, Pl	0.30	0.57	0.42	8.970
S-14	Ilt+Kln+Qz	Mnt+Chl (m)+Kln	Ab, Hem	0.20	0.46	0.38	-
S-12-3	Ilt+Qz	Mnt+Chl(?)+Kln	Carb, Pl	0.20	1.28	0.38	8.999
S-16	Ilt+Qz	Mnt+Chl+Kln	Carb, Pl	0.25	0.22	0.24	9.006
S-19	Ilt+Qz	Mnt+Chl(?)+Kln	Carb, Pl	0.30	0.93	0.32	9.026
G-2	Ilt	Kln+Qz	Fap, Pl, Hem	0.20	0.14	0.28	8.909
G-8	Ilt	Kln+Qz	Fap, Pl, Carb, Px	0.20	0.28	0.31	8.884
G-5	Ilt	Kln+Qz	Pl, Carb	0.15	0.16	0.25	8.921
K-2	Ilt	Mnt+Chl+Qz	Pl, Carb	0.14	0.67	0.31	8.999
Lokapur Subgroup							
P-6	Mnt+Chl+Ilt	Qz	Hem., Pl	0.20	-	0.37	8.871
P-8	Ilt+Mnt+Chl	Qz	Hem., Pl	0.20	-	0.47	8.909
T-11	Ilt	Mnt+Kln+Qz	Mnt+Ilt (m), Fap Mnt+Chl (m), Pl	0.20	0.42	0.36	9.006
T-10	Ilt	Mnt+Kln+Qz	Carb, Pl	0.20	0.15	0.22	9.036
T-8	Ilt+Mnt	Kln+Qz	Mnt+Chl (m), Mnt+Ilt (m), Pl	0.20	0.30	0.32	8.974
T-6	Ilt+Mnt+Kln	Qz	Mnt+Ilt (m), Pl, Mnt+Chl(m), Carb	0.25	0.34	0.40	8.935

Index for samples: T - Manoli shales; K, G, and S - Govindakoppa; D - Dadanhatti; P - Hebbal.
Index for minerals: Mnt - Montmorillonite; Ilt - Illite; Kln – Kaolinite; Chl - Chlorite; (m) - Mixed layers; Fap - Fluroapatite; Pl - Plagioclase; Hem - Hematite; Px - Pyroxene; Qz - Quartz; Carb - Carbonate minerals; K/I - Kaolinite/Illite ratio; IC - Illite crystallinity in $^{\circ}\Delta 2\theta$.

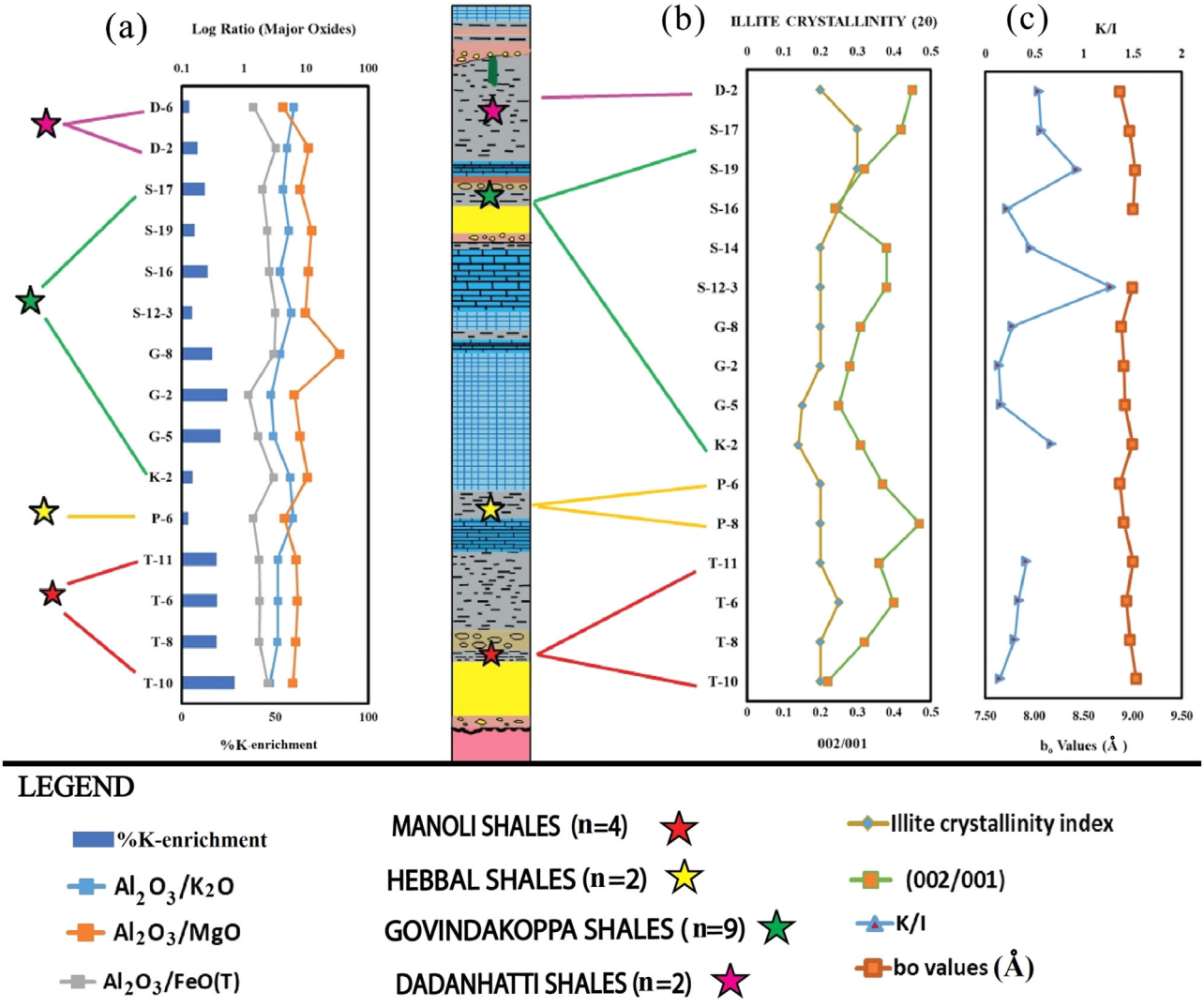

Fig. 3. (a) Major oxide and K% variation within shales collected from four formations. (b) IC (Illite crystallinity index) and 002/001 variation in shales. (c) K/I, b_o values, and (Å) variations in shales.

Table 3
DTA data of mineral assemblages of the Kaladgi shales.

Sample No.	Endothermic reactions in°C	Exothermic reactions in°C
Upper shales		
D-2	562 [2.5] (Ilt+Kln+Qz)	945 [0.2] (Mnt)
	715 [0.5] (Mnt)	962 [0.3] (Kln)
S-12-3	560 [0.5] (Ilt+Qz)	845 [0.5] (Chl+Mnt)
	615 [0.6] (Chl)	975 [0.3] (Kln+Mnt)
	778 [0.2] (Ilt)	
	815 [0.3] (Chl+Mnt)	
	875 [0.5] (Ilt)	
S-17	560 [1.6] (Ilt+Qz)	280 [0.2] (Ilt)
	890 [1.0] (Ilt)	415 [0.2] Couplet
		465 [0.2] (Ilt)
		968 [0.5] (Kln)
G-8	535 [0.03] (Ilt+Kln+Qz)	430 [0.5] (Ilt)
	550 [0.5] (Kln+Ilt+Qz)	505 [0.3] (Ilt)
		950 [0.05] (Kln)
Lower shales		
T-11	530 [0.05] (Qz)	435 [0.5] (Ilt)
	695 [0.3] (Mnt)	505 [0.3] (Ilt)
	880 [0.4] (Ilt+Chl)	430 [0.2] (Ilt)
T-6	568 [1.6] (Kln+Ilt)	465 [0.3] (Ilt)
	698 [0.8] (Mnt)	836 [0.3] (Chl+Mnt)
	882 [0.3] (Ilt+Chl)	960 [0.5] (Kln)

The index for the samples is the same as in Table 2.
Index for the minerals: Ilt - Illite, Kln - Kaolinite, Mnt - Montmorillonite, Chl - Chlorite, Qz - Quartz.
Values in parentheses indicate Δ T in°C.

in some upper shales (S-17 and G-8). The sample S-12-3, an upper shale, shows a considerable amount of chlorite, exhibited by the characteristic thermal reactions of chlorite's strong endothermic peak at 615°C and an exothermic peak at 845°C. These peaks are noticeably absent in the samples D-2, S-17, and G-8 of the upper shales and T-11 and T-6 of the lower shales.

5. Provenance modeling

The factors contributing to the chemical compositions of clastic sedimentary rocks are the source, weathering history, and post-depositional alteration processes (see Absar, 2021). Physical weathering and/or weak chemical weathering on crystalline igneous and metamorphic rocks is related to a dry climate or strong rate of tectonic uplift. Such processes tend to generate illite, chlorite as well as fine fractions of quartz and feldspar constituting fragments of primary minerals (Liu et al., 2012). The geochemistry of these sediments provides information about the provenance composition. Previous studies by Rao et al. (1999) on Kaladgi shales inferred that the provenance of the basin shifted from mafic to felsic source based on major oxides, trace, and REE compositions of Kaladgi shales. Cr, Fe, Ni, Sc, Co, and Mg are in higher abundance in the Lower Group shales (Bagalkot), indicating mafic sources. In contrast, LILE and LREE are enriched in the upper group shales due to a shift in the provenance.

Based on REE ratios, the provenance modeling Rao et al. (1999) suggested a 60:40 ratio for the mafic to felsic components in the provenance for Kaladgi shales. The earlier modeling results suggested a classical unroofing that indicated uncovering granites after the erosion of Archean TTGs and mafic supracrustals with the progression of sedimentation in the Kaladgi Basin (Rao et al., 1999). Further, they proposed that the LREE enrichment in the shales is due to post-depositional K-metasomatism. However, studies by (Dey et al., 2008b) refuted the idea of K-metasomatism being responsible for LREE enrichment in the shales. Instead, they conclude that excluding K-rich Closepet granites having high LILE and LREE as a source rock is the plausible reason behind the unusually high enrichment of REE observed in these shales.

In this study, we attempted a new provenance modeling approach (after Kasanzu et al., 2008), which includes critical REE ratios like $(La/Yb)_N$, $(La/Sm)_N$, $(Gd/Yb)_N$, and $(Eu/Eu^*)_N$. The major, trace and REE compositions of Kaladgi shales (after Rao et al., 1999) are modeled using the end-member compositions representing the provenance. The following are considered as part of the provenance: TTG (Peninsular Gneisses, Jayananda, et al., 2015), Closepet Granites (Jayananda et al., 2006), and mafic rocks from Hungund-Kushtagi schist belts (Naqvi et al., 2006). The centripetal paleocurrent directions of the basin (George, 1999) corroborate with the consideration of the above end-members as part of the source rocks. Importantly, we have incorporated the K-rich Closepet Granite as one of the end-members in the calculations and modeled the provenance for lower and upper shales separately.

The chondrite normalized REE plots of the Kaladgi shales show a closer resemblance with all the plausible source rocks surrounding the basin. The REE modeling method is based on (Albarède, 2002) mixing calculations to estimate the relative contributions of source rocks for generating the Kaladgi shales. The system O containing several elements (i = 1, ..., m) hosted in phases (j = 1, ..., n), let M_j be the mass of phase j and m_j^i The mass of an element (or species) i hosted in phase j. Then, the composition of species (or element) i in phase j can be mathematically defined as:

$$C_j^i = \frac{m_j^i}{M_j} \quad (1)$$

For the bulk material, mass conservation requires that $M_0 = \sum_{j=1}^{n} M_j$.

Therefore, for a given element i, the proportion of f_j of the phase j is such that: $f_j = M_j/M_0$ and $C_0^i = m_0^i/M_0 = \sum_{j=1}^{n} m_j^i / M_0$ (Albarède, 2002). As described above, the four major rock types that were considered as part of the provenance are Closepet Granites, TTG (Peninsular Gneiss), mafic (high Mg basalt and intermediate volcanics) rocks, and adakites of Greenstone belt (Hungund Kushtagi Greenstone belt). The average REE concentrations of shales and protolith were used for modeling based on important critical ratios $(La/Yb)_N$, $(La/Sm)_N$, $(Gd/Yb)_N$, and $(Eu/Eu^*)_N$ from (Table 4) set in a matrix form and represented in (Table 5). The only difference is that the critical ratios taken are more than Kasanzu et al. (2008) because plausible source rock types are more for the Kaladgi Basin. A total of 24 models for lower and upper shales were created to verify whether all the source rock types contribute significantly to the details of the modeling method and all the model variations (Supplementary Data, Figs. S1 and S2).

The results of the mixing calculation (Table 6a, b) suggest that the various components of the provenance contributed to the Lower Group shale compositions in the following proportions: mafic rocks (high Mg basalt + intermediate volcanics) – 34%, Closepet Granite – 35%, TTG (Peninsular Gneiss) – 20%, Fe-tholeiites – 11 %. On the other hand, the upper shale compositions indicate that source rocks are dominated by Closepet Granite (61%) and intermediate volcanic rocks (39%). The optimal fitting of average REE concentrations of Kaladgi shales is achieved with the help of mass balance calculations using the equation Albarède (2002) given.

$$\mathbf{WR_{mix}} = \alpha C_1 + \beta C_2 + \gamma C_3 + \ldots \quad (2)$$

WR_{mix} refers to the calculated wholerock compositions. The α, β, and γ represent the rock types' proportions; in our case, they are Closepet Granites, TTG (Peninsular Gneiss), mafic (high

Table 4
Average REE compositions of all plausible source rocks of sediments belonging to the Kaladgi Badami Basin.

	Fe basalt (Average) n=2	Stdev	High Mg basalt (Average) n=11	Stdev	Intermediate volcanoes (Average) n=10	Stdev	TTG (Average) n=15	Stdev	Closepet granite (Average) n=17	Stdev
La	7.61	1.48	8.78	14.91	10.88	4.48	32.59	20.59	67.07	38.42
Ce	16.805	6.72	12.73	12.56	17.95	8.08	65.74	43.88	133.98	75.47
Pr	2.29	0.75	4.20	9.81	3.11	3.44	7.69	6.26	15.09	8.55
Nd	12.77	5.50	9.09	8.70	9.32	3.56	31.34	28.32	52.66	29.76
Sm	4.195	1.29	3.67	6.38	2.72	2.04	7.37	7.63	9.76	4.82
Eu	1.34	0.47	0.96	1.23	0.80	0.38	1.48	1.09	1.40	0.93
Gd	5.09	1.17	3.25	4.06	2.66	1.21	7.56	8.47	8.30	3.97
Dy	6.21	1.90	2.80	1.22	2.44	0.66	7.45	8.52	7.90	3.90
Er	3.475	1.04	1.73	1.32	1.79	0.69	4.54	5.13	4.42	2.24
Yb	3.68	0.69	1.63	0.77	1.77	0.48	4.90	5.35	4.50	2.13
Lu	0.47	0.14	0.35	0.51	0.35	0.25	0.75	0.81	0.67	0.31
Eu/Eu*	0.88		0.85		0.90		0.60		0.47	
La/Yb	1.40		3.66		4.19		4.52		9.75	
Gd/Yb	1.12		1.61		1.22		1.25		1.44	
La/Sm	1.13		1.49		2.50		2.76		4.29	

Table 5
Depicting the matrix equation for provenance modeling (a) upper shales (Simikeri Group), (b) lower shales (Lokapur Group).

(a)							
Ratio	**A**	**B**	**C**	**D**			**Upper Shales (Avg)**
$(Eu/Eu^*)_N$	0.85	0.47	0.60	0.90	**A**		0.68
$(La/Yb)_N$	3.01	9.75	4.52	4.19	**B**	=	9.44
$(Gd/Yb)_N$	1.47	1.44	1.25	1.22	**C**		1.49
$(La/Sm)_N$	1.43	4.29	2.76	2.50	**D**		4.38
A= Mafics (High Mg basalts & Fe tholleite); **B=** Granite (potassic); **C=** TTG; **D=** Intermediate volcanics							
(b)							
Ratio	**A**	**B**	**C**	**D**			**Lower Shales (Avg)**
$(Eu/Eu^*)_N$	0.87	0.47	0.60	0.88	**A**		0.75
$(La/Yb)_N$	3.92	9.75	4.52	1.40	**B**	=	11.23
$(Gd/Yb)_N$	1.42	1.44	1.25	1.12	**C**		1.86
$(La/Sm)_N$	1.90	4.29	2.76	1.13	**D**		4.53
A= Mafics (High Mg basalts & Fe tholleite); **B=** Granite (potassic); **C=** TTG; **D** = Fe tholleite							

Mg basalts + Intermediate Volcanic) rocks, and Adakites (Hungund Kushtagi belt) respectively. C_1, C_2, and C_3 are the individual species (elements) in the above source components used in the mixing calculations. The results based on the REE parameters are presented in (Table 6a, b) and (Fig. 4).

6. Discussion

6.1. Inferences from XRD and DTA studies of shales

The Archean granitoids, gneisses, and supracrustal rocks were provenance for the Kaladgi siliciclastic sedimentary rocks. The CIA values of the Kaladgi shales are ~89% indicating that the provenance suffered an intense chemical weathering. The REE modeling indicates that four provenance rock types are mainly contributing, i.e., mafic rocks - 25 %, K-Granite – 35%, TTG – 34%, Adakites – 6% (Fig. 4c). Weathering of mafic rocks form montmorillonite clay minerals, whereas felsic rocks (Granites) usually form kaolinite (Weaver, 1989). The frequency distribution of clay minerals (Fig. 5) indicates that montmorillonite is mainly present in Hebbal and Manoli argillites (Lokapur Subgroup). In contrast, the Govindakoppa and Daddanhatti argillites (Simikeri Subgroup) contain considerably higher kaolinite than the lower shales.

The illite clay mineral is primarily present in the shales from both lower to upper formations. Illite is a significant clay mineral component along with kaolinite and montmorillonite. The illite formation can occur through diagenetic alteration of montmorillonite and kaolinite clay minerals (Velde, 1995). This transformation depends upon the pH of the medium, pore water chemistry, porosity, permeability, temperature, pressure, and possibly time (Weaver, 1989). Further, Chamley (1989) stated that the types of diagenetic transformation or new mineral formation also depends upon the nature of original sediments and burial depth. The dominance of illite and the presence of chlorite in the clay mineral assemblages of Kaladgi shales suggests that they might have been newly formed at the expense of primary clay minerals such as montmorillonite and kaolinite. However, it is suggested that smectite can be transformed into illite, chlorite, and illite-smectite-chlorite (I/S/Chl) mixed layer minerals under diagenetic and low-grade metamorphic conditions by following reactions (Boles and Franks, 1979; Weaver, 1989):

$$\text{Smectite} + K^+ \rightarrow \text{Illite} + \text{Quartz} + OH^- + O^{2-} + \text{metallic cations}$$

or

$$\text{Smectite}\left(Fe^{3+}\right) + \text{Kaolinite} \rightarrow \text{I/S/Chl} + Si^{4+}$$

The illite and chlorite present in the Manoli and Hebbal argillites is possibly due to diagenesis. The abundance of the mineral composition Mnt + Ilt + Chl and mixed-layers attests to such a proposition. The diagenetic formation of illite is facilitated by saline, K ion-enriched, organic poor migrating ground waters through bedding planes, joints, and pore spaces (Eberl, 1993). *In situ* illites can be formed either by illitization of kaolinite or of smectite or both, a feature commonly observed in sediments that witnessed burial diagenesis (*ibid*). The kaolinite and montmorillonite clay minerals readily convert to illite in the presence of K^+ and Na^{2+} ions (Nesbitt and Young, 1989).

Moreover, the illitization of kaolinite is much faster than the illitization of montmorillonite, as suggested by reaction kinetics (Velde, 1995). Hence, the present assemblage in the Kaladgi shales

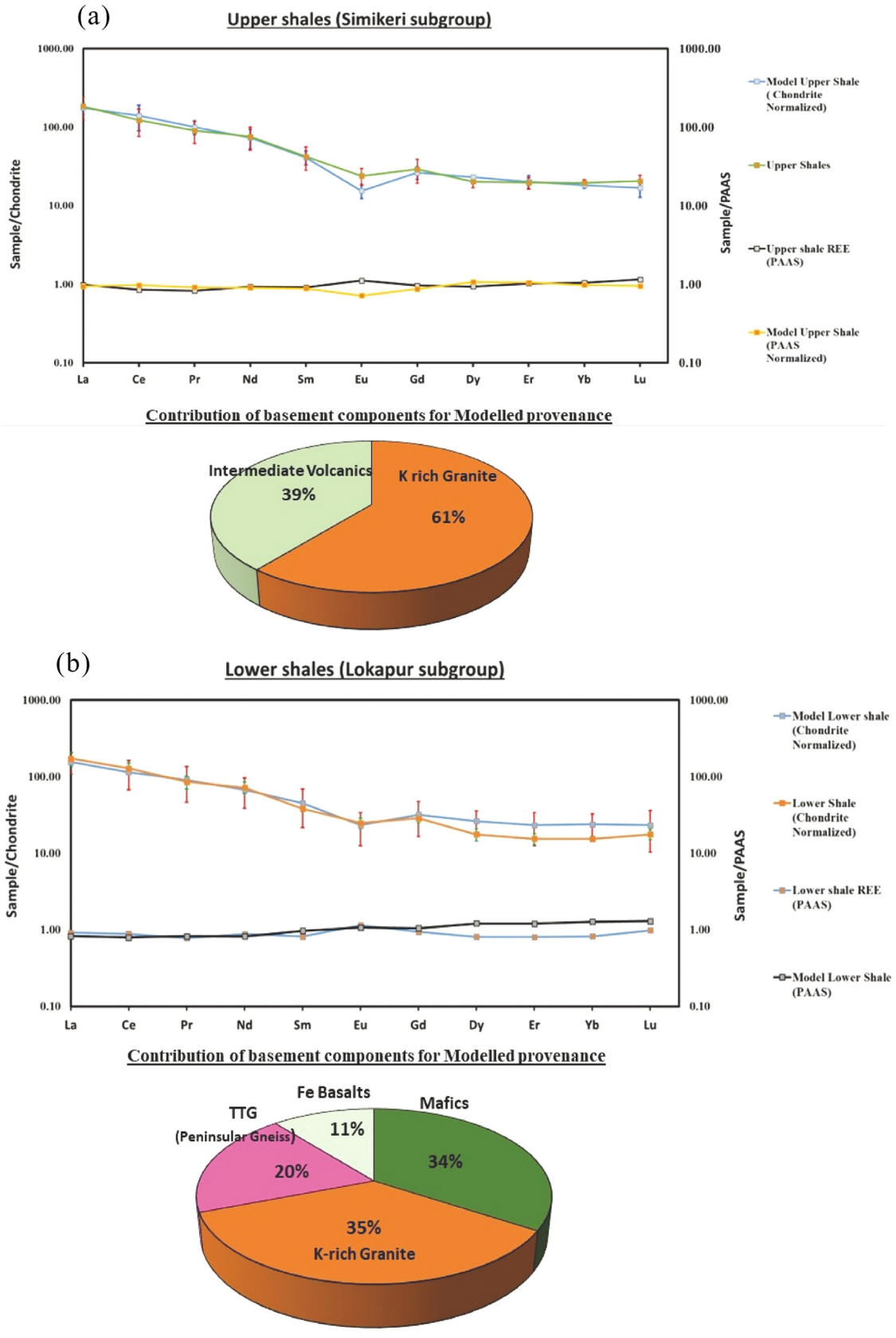

Fig. 4. (a) Comparison between chondrite normalized REE patterns of model shale and average shale of the Kaladgi Basin. The blue and green bands indicate 1σ error for model shale and average Kaladgi shale, respectively. (b) Chondrite normalized REE plots consisting of all the plausible average source rock and average Kaladgi shale (c) Pie chart depicting source rock contribution in the provenance.

Table 6
(a) Mixing modelling results for upper shales (Simikeri Group); (b) Mixing modelling results for lower shales (Lokapur Group).

(a) Mixing modelling results for upper shales (Simikeri Group)				
Source rocks	Mafics* (HK)	Granite (potassic)	TTG	Intermediate volcanics
Model (%)	0	61	0	39
ppm	**Model (upper shale)**	**Average upper Kaladgi shales**		**Variation (%)**
La	41.92	44.00		4.73
Ce	86.02	75.40		14.08
Pr	9.32	8.43		10.53
Nd	33.79	34.77		2.83
Sm	6.11	6.27		2.53
Eu	0.87	1.35		35.66
Gd	5.27	5.82		9.41
Dy	5.71	4.98		14.63
Er	3.25	3.15		3.10
Yb	2.96	3.17		6.47
Lu	0.42	0.51		17.60
Total REE	195.62	187.84		4.14
$(Eu/Eu^*)_N$	0.47	0.68		
$(La/Yb)_N$	9.62	9.44		
$(Gd/Yb)_N$	1.44	1.49		
$(La/Sm)_N$	4.29	4.53		
(b) Mixing modelling results for lower shales (Lokapur Group)				
Source rocks	Mafics* (HK)	Granite (potassic)	TTG	Fe tholeiite
Model (%)	34	35	20	11
ppm	**Model (lower shales)**	**Average lower Kaladgi shales**		**Variation (%)**
La	36.76	40.83		9.97
Ce	70.25	78.50		10.50
Pr	8.40	7.93		5.93
Nd	30.72	32.92		6.67
Sm	6.70	5.63		18.88
Eu	1.30	1.40		6.59
Gd	6.36	5.67		12.10
Dy	6.45	4.31		49.62
Er	3.71	2.48		49.81
Yb	3.84	2.47		55.52
Lu	0.57	0.43		31.50
Total REE	175.07	182.58		4
$(Eu/Eu^*)_N$	0.61	0.75		
$(La/Yb)_N$	6.50	11.23		
$(Gd/Yb)_N$	1.34	1.86		
$(La/Sm)_N$	3.43	4.53		

* Mafics include High-Mg basalts and intermediate volcanics from the Hungund-Kushtagi greenstone belt.

Table 7
Average abundances and ratios of some major elements significant for understanding the diagenetic origin of illite and chlorite in the shales of the Bagalkot Group.

		Upper shales (SSG)			Lower shales (LSG)
Oxides/Ratios	Range	Average (11)		Range	Average (5)
Al_2O_3	13.6-21.4	18.78 ±	2.90	16.7-17.97	17.24 ± 0.43
MgO	0.6-3.8	1.87 ±	0.82	2.5-3.73	2.80 ± 0.48
K_2O	2.5-5.6	4.23 ±	0.85	2.7-6.6	4.84 ± 1.23
FeO(t)	6.6-11.5			7.1-11.8	
Al_2O_3/K_2O		4.63 ±	1.14		3.86 ± 1.21
Al_2O_3/MgO		13.08 ±	8.96		6.34 ± 1.00
Al_2O_3/FeO(t)		2.43 ±	0.71		1.83 ± 0.32

is more likely represented by Ilt+Chl. Three Govindakoppa argillite samples (G-2, G-8, and G-5) contain only kaolinite+illite, and the proportion of illite is much more than kaolinite in these samples. The average kaolinite/illite ratio is high in the Simikeri Subgroup shales. Shales belonging to Manoli and Hebbal argillites have a lower ratio, around 0.33, which indicates a high amount of illite-rich shales than those belonging to the upper formations (Fig. 3b). Such an increase in illite contents is partly due to the illitization of kaolinite with the increasing effect of burial diagenesis. Major oxide ratios such as Al_2O_3/K_2O, Al_2O_3/MgO, Al_2O_3/FeO (t) decrease from 4.36 to 3.28, 12.51 to 6.81, and 2.49 to 1.83 (Table 7), respectively, from younger to older formations pointing towards authigenic growth of these minerals (Fig. 3a). The higher illite proportion in Kaladgi shales indicates that the activity of K^+ ions is higher than that of Mg^{2+} ions in the pore water. Therefore, the deeply buried sediments show an increase in illite due to changes in pressure and temperature. The persistence of montmorillonite and kaolinite in Proterozoic shales along with illite and chlorite suggests that illitization of these minerals was not complete, possibly due to (i) slow transformation rates, (ii) relatively low activity amongst – Ca^{2+}, Mg^{2+}, Fe^{2+}, K^+, in an alkaline medium with pH ranging from 7.5-9.0 (Velde, 1995), and (iii) low porosity and permeability. The presence of smectite in clay mineral assemblage indicates higher silica activity in pore waters. In a low pH environment, silica is unstable, indicating that pore water was more alkaline and had moderate to high pH values.

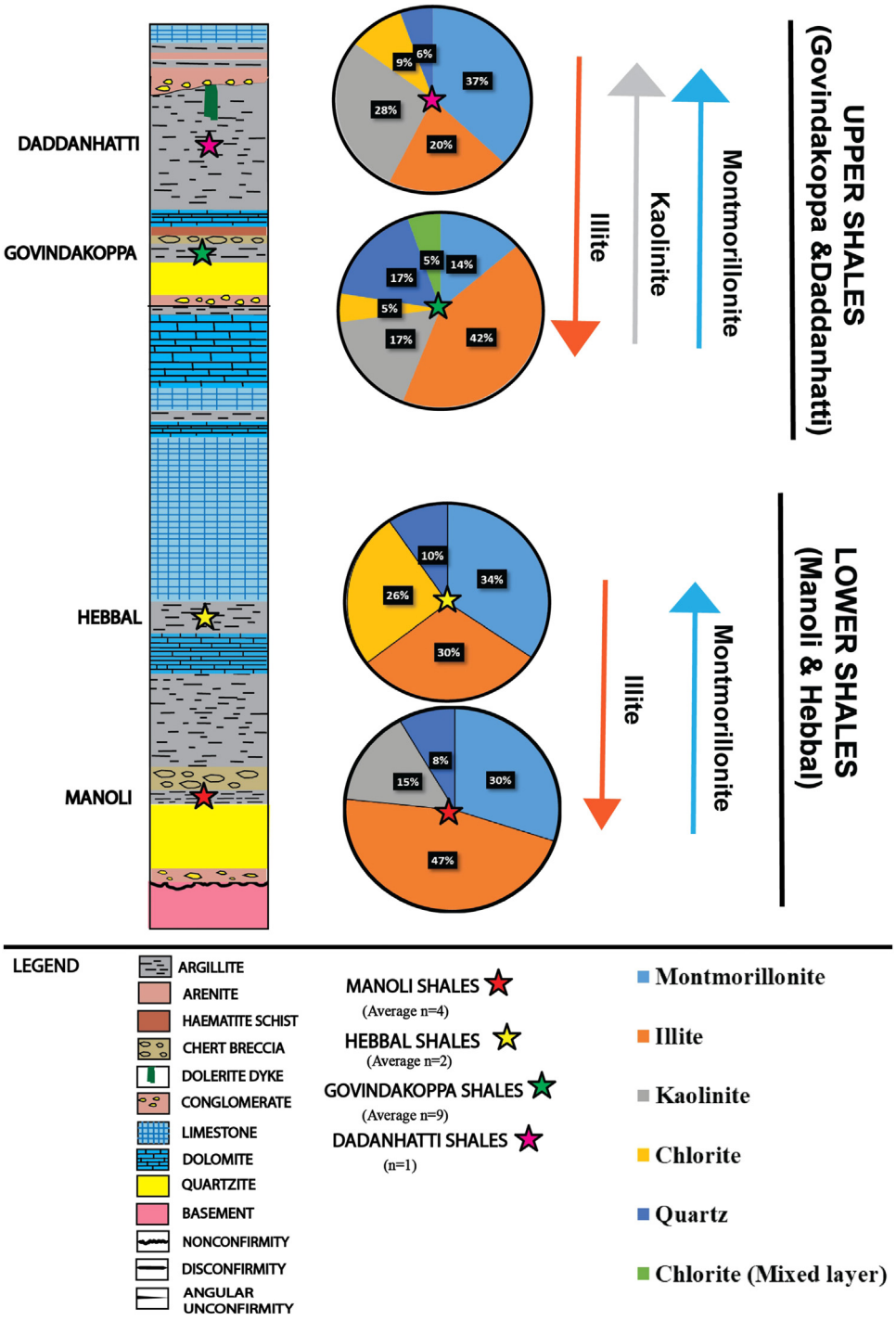

Fig. 5. Pie charts depicting average clay mineral contents based on XRD analysis in lower and upper shales. Each pie chart represents the average clay contents in shales of various formations, with n representing the number of samples. The arrows of different colors represent increasing directions of montmorillonite (blue), illite (orange), and kaolinite (grey) within upper and lower shales.

Chlorite is the other clay mineral in minor to trace amounts in all the shales belonging to both upper and lower formations (Table 2). The chlorite values of the M/Chl clays are mainly attributed to the incomplete transformation of montmorillonites to chlorites at different burial depths, possibly under the influence of Mg^{2+} activity. The complete alteration of smectite to diagenetic ferriferous chlorite is rare even in Mg-rich environments (Chamley, 1989). The formation of Mg-chlorite also occurs in slightly higher grades of metamorphism. However, Hower et al. (1975) pointed out that a part of Mg and Fe released during the transformation of smectite to illite could favor the formation of diagenetic chlorite as a direct by-product. From the preceding discussion, it can be suggested that chlorites and illites in Bagalkot Group of shales were formed due to the transformation of montmorillonite by burial diagenesis.

The DTA data of two samples from the lower Simikere Subgroup show endothermic reaction temperatures indicative of the presence of illite, chlorite, montmorillonite, and kaolinite. The endothermic temperature of ~695°C indicates the Mnt, and ~568 and 880°C point to the Kln + Ilt and Ilt + Chl mixture in lower

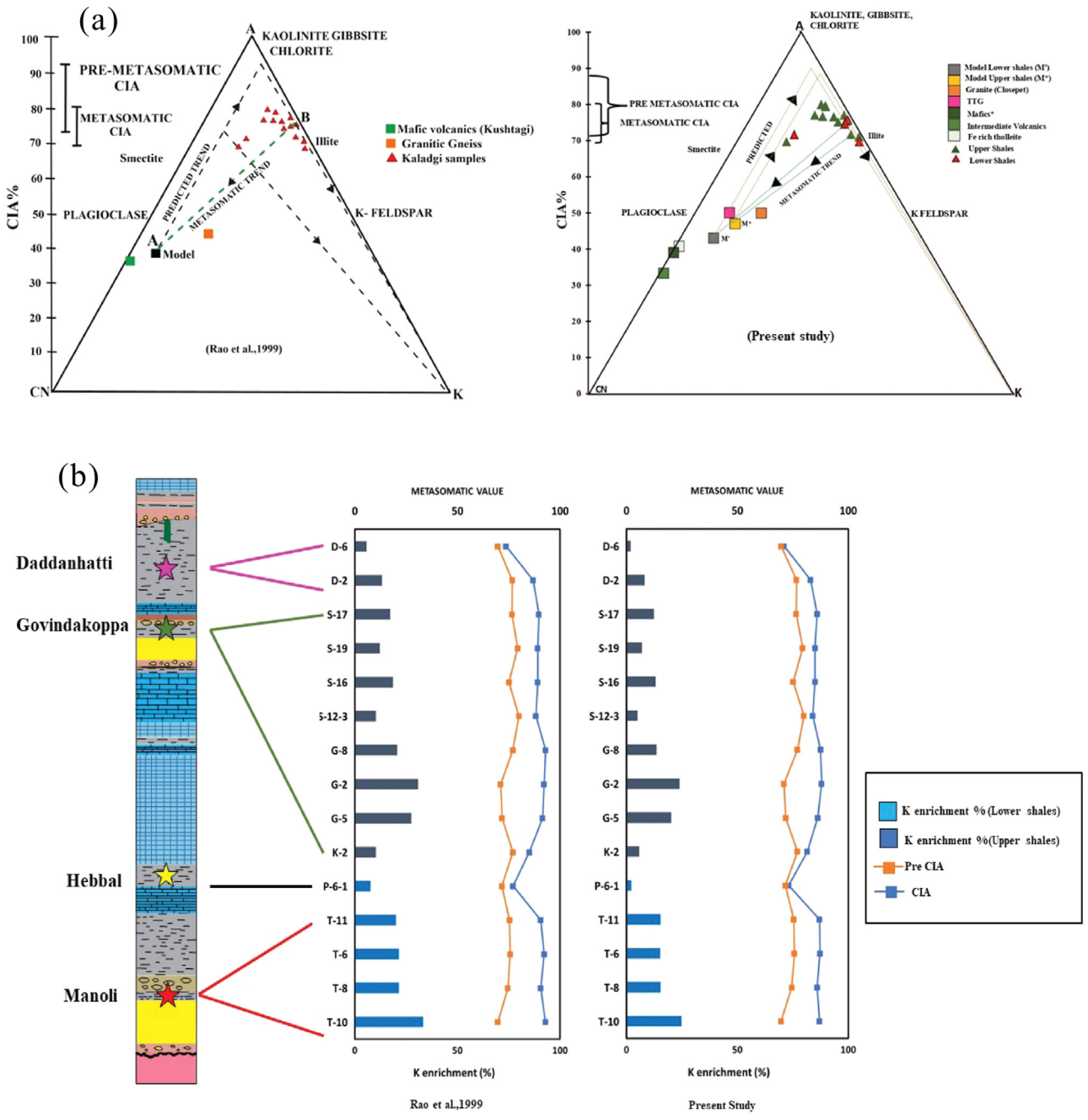

Fig. 6. (a) The A-CN-K plot of Kaladgi shales. The model provenance of Rao et al. (1999) and the present study are shown separately; (b) The CIA values and pre-metasomatic CIA values of the previous and current study are shown. The main difference is that the present research involves K-rich granites in the provenance, hence the lesser difference between CIA and pre-metasomatic CIA values. The K-enrichment (%), which is the difference between pre-metasomatic CIA and CIA values, is also shown.

shales. The exothermic reaction temperatures of 435 to 505°C indicate Ilt, 960°C to Kln, and 836°C to Chl + Mnt mixture. Upper shale members' endo- and exo-thermic reaction temperatures show a consistent presence of Ilt, Kln, Ilt + Kln + Qz, and Kln + Ilt. The results of this study are consistent with earlier DTA study on Kaladgi shales (Chandrasekhara Gowda et al., 1978).

6.2. REE modeling and K-metasomatism

The illitization of montmorillonite and kaolinite as indicated by XRD data and the presence of illite in all the shales attest to the post-depositional alteration effects. Earlier studies (Govinda Rajulu and Nagaraja, 1967) reported the presence of K-metasomatism through diagenetic feldspathization of Lower Kaladgi arkoses. The potassic feldspathization observed in conglomerates and arenites belonging to the Kaladgi Supergroup is also reported . The difference between present CIA values and pre-metasomatic CIA values in shales is significant, indicating a high K influx (Rao et al., 1999), which justifies previous evidence of diagenetic feldspathization. The estimated provenance of the present study and the compositions of shales are plotted in the A-CN-K diagram (Fig. 6a) to evaluate the effects of K-metasomatism. The increased percentage in pre-metasomatic CIA values is also estimated, along with % K enrichment (after Fedo et al., 1995). The difference in our calcula-

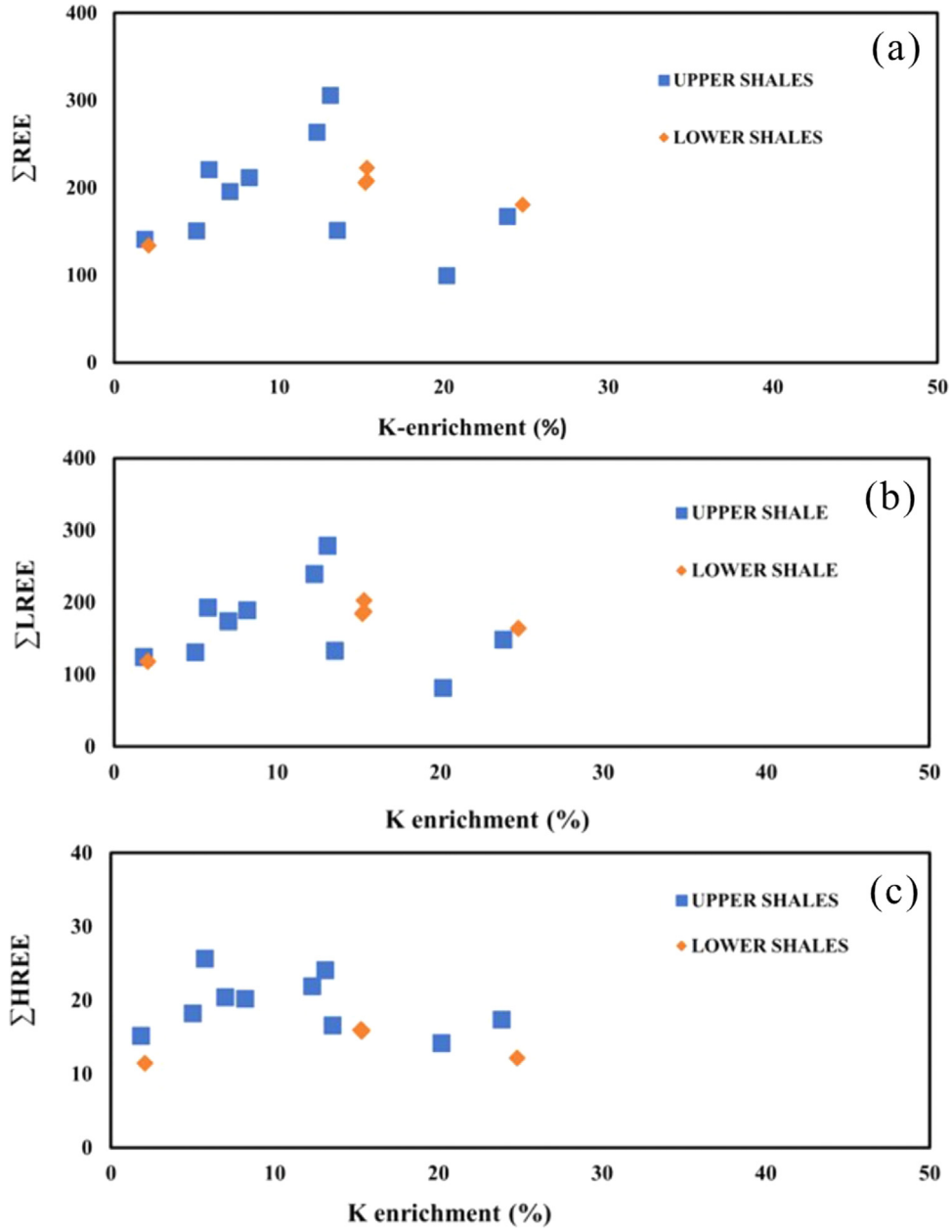

Fig. 7. K enrichment (%) vs. (a) ΣREE; (b) ΣLREE; (c) ΣHREE.

tion is that we considered K-rich granites part of the provenance, while it was excluded in the earlier model (Rao et al., 1999). The average difference between the pre-metasomatic CIA and metasomatic CIA values comprising both upper shales and lower shales is 9.1 ± 5.1. The average value for upper shales is 8.3 ± 4.9, while for lower shales, it is 10.7 ± 5.7, indicating the lower shales are more affected by K-metasomatism. The average K enrichment (%) in both lower and upper shales is 12.2 ± 7.3%, with a maximum value of 24% observed in the lower shales (Manoli and Hebbal). The increased percentage values obtained in the present study are lesser than those reported by Rao et al. (1999; Fig. 6b). Such a difference is due to consideration of K-feldspar rich Closepet Granite as part of the provenance in our modeling. Further, Rao et al. (1999) interpreted that the increased K enrichment % values are positively correlated with LREE, suggesting the addition of LREE in shales due to K-metasomatism.

In the present study, the modeled provenance and the average shale compositions in the cases of both lower and upper shales show an excellent match (Fig. 4a, b), indicating that there may not be a need to invoke additional sources of LREE. The plot showing correlation between % K enrichment and the REE contents (Fig. 7a, b) indicates that a few upper shale samples positively correlate with ΣLREE and ΣREE, while lower shales show a scatter. The shale samples with <10% values in K-enrichment are more positively correlated with ΣLREE and ΣREE, while the shales with >10% of K-enrichment do not show any correlation with REE contents (Fig. 7a, b). Kaolinites tend to fractionate LREE (Galán et al., 2007; da Silva et al., 2017; Andrade et al., 2022). It is further demonstrated that most REE^{3+} is adsorbed as 8–9-fold hydrated outer-sphere complexes to kaolinite (Borst et al., 2020). It is important to note here that the XRD studies indicate upper shales contain more kaolinite, which is possibly due to the increased contribu-

tion of the K-feldspar-rich granites in the provenance. The XRD analysis and the lower increase percentage in CIA values in upper shales point out the persistence of kaolinites in them. We suggest that the observed positive correlation between % K-increase and ΣLREE in upper shales is due to kaolinite that would have fractionated more LREE. The lower shales, on the other, have more contribution from mafic sources and have more montmorillonite. The difference in chemical compositions of upper and lower shales in terms of mafic and felsic source indicators points out that the latter has more contribution from mafic sources (Rao et al., 1999). Our modeling of the lower and upper shale REE contents revealed the distinction in the source rock compositions. While lower shales are derived from a provenance dominated by TTG and mafic rocks (65%), the upper shale compositions indicate that the granites are significantly present (61%). Our modeling thus corroborate with the classical unroofing of greenstones exposing the K-rich granites later during the sedimentation as proposed earlier (Rao et al., 1999). However, we suggest that hydrothermal or fluid activity during K-metasomatism is not responsible for the enrichment of LREE in Kaladgi shales. The ability of kaolinites to fractionate LREEs more in the upper shales is the reason for the overall enrichment of REEs and the observed LREE enrichment. Capacity of kaolinite in rare earth ion-adsorption in acidic and basic environments reported in south China (Feng et al., 2021) is also supporting the idea of K-enrichment.

The high amount of K ions in the pore waters could be due to the dissolution of K feldspar and detrital illite (Miliken, 2003). The presence of K-rich Granite in provenance corroborates the involvment of K feldspar dissolution. Further, the local contribution of K from sandstone lying above the shales might have contributed K content in these shales (Thyne, 2001). The Possibility of K-enrichment and illite formation due to mat structures (Aubineau et al., 2019) in shales cannot be ruled out from Kaladgi-Badami basins. The shale algal mat structures are not reported yet in the Kaladgi shales. However, light hydrocarbons are reported from the soils (derived from these shales in a surface geochemical prospecting survey) conducted within the Kaladgi Basin (Kalpana et al., 2010), suggesting the presence of organic molecules in these shales.

7. Conclusions

- The XRD studies of Kaladgi shales suggest that the clay mineral assemblage of lower shales (Manoli and Hebbal) is consistent with their derivation from more mafic sources. In contrast, the upper shales (Govindakoppa and Daddanhatti) were derived from more felsic sources. Montmorillonite and kaolinite are the primary clay minerals present in the shales during sedimentation. The illite and chlorite are by-products of diagenesis in an alkaline environment controlled by cations of pore water. The montmorillonite and kaolinite persistence in Proterozoic Kaladgi shales is due to sluggish transformation rates and incomplete conversion of the primary clay minerals during post-depositional alteration.
- The geochemical modeling results suggest distinct provenance for lower and upper shales. The lower shales derived from a more mafic source having TTGs and mafic rocks up to 65%, and the upper shales derived from a provenace consisting 61% granites. Our modeling suggests a significant contribution from the K-enriched Closepet Granite, especially in the case of upper shales. Further, the results support a classical unroofing, where TTG-greenstones were eroded, leading to the exposure of K-rich granites subsequently, with the progression of sedimentation from lower to upper formations in the Kaladgi Basin.
- The correlation between K-enrichment and LREE is attributed to a higher abundance of kaolinites in the upper shales.

CRediT author statement

Pronoy Roy: writing of the initial draft, geochemical modeling
G. Parthasarathy: Analysis, supervision, revision, conceptualization
Bulusu Sreenivas: Conceptualization, edit, final draft preparation

Supplementary Data

Fig. S1. Summary of Chondrite normalized REE plots consisting of all the models and the average upper Kaladgi shales.

Fig. S2. Summary of Chondrite normalized REE plots consisting of all the models and the average lower Kaladgi shales.

Declaration of Competing Interest

The authors declare that they have no known competing financial interests or personal relationships that could have appeared to influence the work reported in this paper.

Acknowledgments

The authors acknowledge Dr. V.M. Tiwari, Director, CSIR-NGRI, for his permission and encouragement. P.R. acknowledges UGC for Senior Research Fellowship. The work has been carried out as part of the Ministry of Earth Sciences, Government of India sponsored project no. MoES/P.O.(Geo)/99(i)2017. This contribution commemorates the 80th birthday of Dr. R. Srinivasan, who has been a doyen of Precambrian sedimentology and a mentor to G.P. and B.S. We thank the reviewers, Prof. Nurul Absar and Prof. J.P. Shrivastava, for their insightful comments. Authors thank Prof. M. Santosh for the support and encouragement. G.P. is grateful to National Institute for Advanced Studies, Bangalore, and Indian National Science Academy, New Delhi for the support.

Supplementary materials

Supplementary material associated with this article can be found, in the online version, at doi:10.1016/j.geogeo.2022.100133.

References

Absar, N., Nizamudheen, B.M., Augustine, S., Managave, S., Balakrishnan, S., 2016. C, O, Sr and Nd isotope systematics of carbonates of Papaghni sub-basin, Andhra Pradesh, India: Implications for genesis of carbonate-hosted stratiform uranium mineralisation and geodynamic evolution of the Cuddapah basin. Lithos 263, 88–100.

Absar, N., 2021. Mineralogy and geochemistry of siliciclastic Miocene Cuddalore Formation, Cauvery Basin, South India: implications for provenance and paleoclimate. J. Palaeogeogr. 10, 602–630. doi:10.1016/j.jop.2021.11.006.

Albarède, F., 2002. Introduction to Geochemical Modelling. Cambridge University Press, p. 543.

Andrade, G.R.P., Cuadros, J., Barbosa, J.M.P., Vidal-Torrado, P., 2022. Clay minerals control rare earth elements (REE) fractionation in Brazilian mangrove soils. CATENA 209, 105855. doi:10.1016/j.catena.2021.105855.

Aubineau, J., El Albani, A., Bekker, A., Somogyi, A., Bankole, O.M., Macchiarelli, R., Meunier, A., Riboulleau, A., Reynaud, J.Y., Konhauser, K.O., 2019. Microbially induced potassium enrichment in Paleoproterozoic shales and implications for reverse weathering on early Earth. Nat. Commun. 10 (1), 1–9. doi:10.1038/s41467-019-10620-3.

Bailey, S.W., 1988. Hydrous Phyllosilicates. In: Reviews in Mineralogy, 49. Mineralogical Society of America, p. 725.

Basu, A., Bickford, M.E., 2015. An alternate perspective on the opening and closing of the intracratonic Purana basins in peninsular India. Jour. Geol. Soc. India 85 (1), 5–25. doi:10.1007/s12594-015-0190-y.

Bhaskar Rao, Y.J., Pantulu, G.V.C., Damodara Reddy, V., Gopalan, K., 1995. Time of early sedimentation and volcanism in the Proterozoic Cuddapah Basin, South India: evidence from the Rb–Sr age of Pulivendla mafic sill. In: Devaraju, T.C. (Ed.), Mafic Dyke Swarms of Peninsular India, 33. Geological Society of India Memoir, pp. 329–338.

Boles, J.R., Franks, S.G., 1979. Clay diagenesis in Wilcox sandstone in South Texas: implications of smectite diagenesis on sandstone cementation. J. Sediment. Res. 49, 55–70. doi:10.1306/212F76BC-2B24-11D7-8648000102C1865D.

Borst, A.M., Smith, M.P., Finch, A.A., et al., 2020. Adsorption of rare earth elements in regolith-hosted clay deposits. Nat. Commun. 11, 4386. doi:10.1038/s41467-020-17801-5.

Brasier, M., 2012. Secret Chambers: The Inside Story of Cells and Complex Life. Oxford University Press, p. 211 ISBN 978-0-19-964400-1.
Brown, G., 1961. The X-ray Identification and Crystal Structures of the Clay Minerals. Mineral Society, London, p. 544.
Buick, R., Des Marais, D.J., Knoll, A.H., 1995. Stable isotopic compositions of carbonates from the Mesoproterozoic Bangemall Group, northwestern Australia. Chem. Geol. 123, 153. doi:10.1016/0009-2541(95)00049-R.
Cawood, P.A., Hawkesworth, C.J., 2014. Earth's middle age. Geology 42 (6), 503–506. doi:10.1130/G35402.1.
Chamley, H., 1989. Clay sedimentology. Springer Verlag, Berlin, p. 623.
Chandrasekhara Gowda, M.J., Venugopal, J.S., Govindarajulu, B.V., 1978. Differential thermal analysis and thermogravimetric studies of the Kaladgi (Precambrian) argillites, Karnataka. Proc. Indian Acad. Sci., A (E & P Sciences) 87, 101–107. doi:10.1007/BF03182100.
Collins, A., Patranabis-Deb, S., Alexander, E., Bertram, C., Falster, G., Gore, R., Mackintosh, J., Dhang, P., Saha, D., Payne, J., Jourdan, F., Backé, G., Halverson, G., Wade, B., 2015. Detrital mineral age, radiogenic isotopic stratigraphy and tectonic significance of the Cuddapah Basin, India. Gondw. Res. 28 (4), 1294–1309.
Cullers, R.L., Podkovyrov, V.N., 2000. Geochemistry of the Mesoproterozoic Lakhanda shales in southeastern Yakutia, Russia: implications for mineralogical and provenance control, and recycling. Precamb. Res. 104 (1-2), 77–93. doi:10.1016/S0301-9268(00)00090-5.
da Silva, Y.J.A.B., do Nascimento, C.W.A., Biondi, C.M., van Straaten, P., de Souza Júnior, V.S., da Silva, Y.J.A.B., dos Santos, C.A., de Araújo, J.D.C.T., 2017. Influence of metaluminous granite mineralogy on the rare earth elements geochemistry of rocks and soils along a climosequence in Brazil. Geoderma 306, 28–39. doi:10.1016/j.geoderma.2017.06.031.
Dey, S. 2015. Geological history of the Kaladgi-Badami and Bhima Basins, South India: Sedimentation in a Proterozoic intracratonic setup. In R. Mazumder, and P. G. Eriksson (Eds.), Precambrian basins of India: Stratigraphic and tectonic context (ed., Vol. 43) (pp. 283–296). Geological Society of London, Memoir. doi:10.1144/M43.19.
Dey, S, Rai, A.K., Chaki, A., 2008a. Widespread arkose along the northern margin of the Proterozoic Kaladgi basin, Karnataka: Product of uplifted granitic source of K-Metasomatism. J. Geol. Soc. India 71 (1), 79–88.
Dey, S., Rao, R.G., Veerabhaskar, D., Chaki, A., Baidya, T.K., 2008b. Geochemistry of shales from the Proterozoic intracratonic Kaladgi-Badami Basin, Karnataka, southern India as an Indicator of palaeoweathering and evolution of the Dharwar Craton. J. Geol. Soc. India 71 (4), 483–501.
Eberl, D.D., 1993. Three zones for illite formation during burial diagenesis and metamorphism. Clay. Clay Miner. 41, 26–37. doi:10.1346/CCMN.1993.0410103.
Eriksson, P.G., Condie, K.C., Tirsgaard, H., Mueller, W.U., Altermann, W., Miall, A.D., Aspler, L.B., Catuneanu, O., Chiarenzelli, J.R., 1998. Precambrian clastic sedimentation systems. Sediment. Geol. 120 (1-4), 5–53. doi:10.1016/S0037-0738(98)00026-8.
Fedo, C.M., Nesbitt, H.W., Young, G.M., 1995. Unraveling the effects of potassium metasomatism in sedimentary rocks and paleosols, with implicationsfor paleoweathering conditions and provenance. Geology 23, 921–924.
Feng, X., Onel, O., Council-Troche, M., Noble, A., Yoon, R.H., Morris, J.R., 2021. A study of rare earth ion-adsorption clays: the speciation of rare earth elements on kaolinite at basic Ph. Appl. Clay Sci. 201, 105920. doi:10.1016/j.clay.2020.105920.
Galán, E., Fernández-Caliani, J.C., Miras, A., Aparicio, P., Márquez, M.G., 2007. Residence and fractionation of rare earth elements during kaolinization of alkaline peraluminous granites in NW Spain. Clay Minerals 42 (3), 341–352. doi:10.1180/claymin.2007.042.3.07.
George, T.S., 1999. Sedimentology of Kaladgi basin. In: Field workshop on integrated evolution of the Kaladgi and Bhima basins. Geol. Soc. India, Bangalore, pp. 13–17.
Gilleaudeau, G.J., Kah, L.C., 2013. Carbon isotope records in a Mesoproterozoic epicratonic sea: Carbon cycling in a low-oxygen world. Precamb. Res. 228, 85–101.
Govinda Rajulu, B.V., Nagaraja, H.R., 1967. Authigenic feldspars from the Lower Kaladgi Arkoses of Jamkhandi, Mysore State, India. J. Sed. Res. 37 (2), 707–709. doi:10.1306/74D71776-2B21-11D7-8648000102C1865Dc.
Hesse, R., Dalton, E., 1991. Diagenetic and low-grade metamorphic terranes of Gasspe Peninsula related to geologic structure of the Tectonic Acadian Orogenic belts Quebec, Appalachians. Jour. Met. Geol. 9, 775–790. doi:10.1111/j.1525-1314.1991.tb00565.x.
Holland, H.D., 2006. The oxygenation of the atmosphere and oceans. Phil. Trans. Roy. Soc. B: Biol. Sci. 361 (1470), 903–915.
Hower, J., Eslinger, E.V., Hower, M.E., Terry, G.A., 1975. Mechanism of burial metamorphism of argillaceous sediments I Mineralogical and Chemical evidence. Geol. Soc. Am. Bull. 87, 727–757. doi:10.1130/0016-7606(1976)87⟨725:MOBMOA⟩2.0.CO;2.
Jaya Prakash, A.V., Sundaram, V., Hans, S.K., Mishra, N, 1987. Geology of the Kaladgi Badami Basin, Karnataka. Geol. Soc. Ind. Mem. 6, 201–225.
Jayananda, M., Chardon, D., Peucat, J.J., Fanning, C.M., 2015. Paleo-to Mesoarchean TTG accretion and continental growth in the western Dharwar craton, Southern India: constraints from SHRIMP U–Pb zircon geochronology, whole-rock geochemistry and Nd–Sr isotopes. Precamb. Res. 268, 295–322. doi:10.1016/j.precamres.2015.07.015.
Jayananda, M., Chardon, D., Peucat, J.J., Capdevila, R., 2006. 2.61 Ga potassic granites and crustal reworking in the western Dharwar craton, southern India: tectonic, geochronologic and geochemical constraints. Precamb. Res. 150 (1-2), 1–26. doi:10.1016/j.precamres.2006.05.004.
Jha, S.K., Shrivastava, J.P., Bhairam, C.L., 2012. Clay mineralogical studies on Bijawars of the Sonrai Basin: palaeoenvironmental implications and inferences on the Uranium mineralization. J. Geol. Soc. India 79, 117–134.
Joy, S., Patranabis-Deb, S., Saha, D., Jelsma, H., Maas, R., Söderlund, U., Tappe, S., Linde, G., Banerjee, A., Krishnan, U., 2019. Depositional history and provenance of cratonic "Purana" basins in Southern India: a multipronged geochronology approach to the Proterozoic Kaladgi and Bhima basins. Geol. J. 54, 2957–2979.
Kale, V.S., 2016. Proterozoic basins of Peninsular India: status within the global Proterozoic systems. Proc. Ind. Nat. Sci. Acad. 82 (3), 461–477.
Kale, V.S., Phansalkar, V.G., 1991. Purana basins of peninsular India: a review. Basin Res 3 (1), 1–36.
Kalpana, M.S., Patil, D.J., Dayal, A.M., Raju, S.V., 2010. Near surface manifestation of hydrocarbons in Proterozoic Bhima and Kaladgi Basins: Implications to hydrocarbon resource potential. Jour. Geol. Soc. India 76 (6), 548–556.
Karhu, J.A., Holland, H.D., 1996. Carbon isotopes and the rise of atmospheric oxygen. Geology 24 (10), 867–870. doi:10.1130/0091-7613.
Kasanzu, C., Maboko, M.A., Manya, S., 2008. Geochemistry of fine-grained clastic sedimentary rocks of the Neoproterozoic Ikorongo Group, NE Tanzania: Implications for provenance and source rock weathering. Precamb. Res. 164 (3-4), 201–213. doi:10.1016/j.precamres.2008.04.007.
Kisch, H.J., 1991. Illite crystallinity recommendations on sample preparation, X-ray diffraction settings and interlaboratory samples. Jour. Met. Geol. 9, 665–670.
Knoll, A.H., Hayes, J.M., Kaufman, A.J., Swett, K., AU - Lambert, I.B., 1986. Secular variation in carbon isotope ratios from Upper Proterozoic successions of Svalbard and East Greenland. Nature 321, 832–838.
Krumm, H., Buggish, W., 1991. Sample Preparation effects on Illite crystallinity measurement: grain size gradation and particle orientation. Jour. Met. Geol. 9, 671–677.
Lyons, T.W., Reinhard, C.T., Planavsky, N.J., 2014. The rise of oxygen in Earth's early ocean and atmosphere. Nature 506, 307–315.
Liu, Z., Wang, H., Hantoro, W.S., Sathiamurthy, E., Colin, C., Zhao, Y., Li, J., 2012. Climatic and tectonic controls on chemical weathering in tropical Southeast Asia (Malay Peninsula, Borneo, and Sumatra). Chem. Geol. 291, 1–12. doi:10.1016/j.chemgeo.2011.11.015.
Mazumder, R., Eriksson, P.G., 2015. Precambrian basins of India: stratigraphic and tectonic context. Geol. Soc. Lond. Mem. 43 (1), 1–4. doi:10.1144/M43.1.
McCulloch, M.T., Wasserburg, G.J., 1978. Sm-Nd and Rb-Sr Chronology of Continental Crust Formation: times of addition to continents of chemically fractionated mantle-derived materials are determined. Science 200 (4345), 1003–1011.
Milliken, K.L., 2003. Late diagenesis and mass transfer in sandstone shale sequences. Treatise on Geochemistry, Volume 7. Editor: Fred T. Mackenzie. Executive Editors: Heinrich D. Holland and Karl K. Turekian. pp. 407. ISBN 0-08-043751-6. Elsevier, 2003., p.159–190.
Mishra, M., Sen, S., 2012. Provenance, tectonic setting and source-area weathering of Mesoproterozoic Kaimur Group, Vindhyan Supergroup, Central India. Geol. Act. 283–293.
Mukherjee, M.K., Das, S., Modak, K., 2016. Basement–cover structural relationships in the Kaladgi Basin, southwestern India: indications towards a Mesoproterozoic gravity gliding of the cover along a detached unconformity. Precamb. Res 281, 495–520. doi:10.1016/j.precamres.2016.06.013.
Mukherjee, M.K., Modak, K., Ghosh, J., 2019. Illite crystallinity index from the Mesoproterozoic sedimentary cover of the Kaladgi basin, southwestern India: Implications on crustal depths of subsidence and deformation. J. Earth Syst. Sci. 128, 101. doi:10.1007/s12040-019-1124-7.
Naqvi, S.M., Khan, R.M.K., Manikyamba, C., Mohan, M.R., Khanna, T.C., 2006. Geochemistry of the NeoArchaean high-Mg basalts, boninites and adakites from the Kushtagi–Hungund greenstone belt of the Eastern Dharwar Craton (EDC); implications for the tectonic setting. J. Asian Earth Sci. 27 (1), 25–44. doi:10.1016/j.jseaes.2005.01.006.
Nesbitt, H.W., Young, G.M., 1989. Formation and diagenesis of weathering profiles. J. Geol. 97 (2), 129–147. doi:10.1086/629290.
Padmakumari, V.M., Rao, V.V.S., Srinivasan, R., 1998. Model Nd and Rb-Sr Ages of the shales of the Bagalkot Group, Kaladgi Supergroup, Karnataka. National Symposium on Late Quaternary Geology and sea level changes. Cochin University, Kochi, p. 70.
Pillai, P.S., Pande, K., Kale, V.S., 2018. Implications of new $^{40}Ar/^{39}Ar$ age of Mallapur Intrusives on the chronology and evolution of the Kaladgi Basin, Dharwar Craton, India. Jour. Earth Syst. Sci. 127 (3), 1–18. doi:10.1007/s12040-018-0940-5.
Planavsky, N.J., Reinhard, C.T., Wang, X., Thomson, D., McGoldrick, P., Rainbird, R.H., Johnson, T., Fischer, W.W., Lyons, T.W., 2014. Low Mid-Proterozoic atmospheric oxygen levels and the delayed rise of animals. Science 346, 635–638.
Radhakrishna, B.P., Naqvi, S.M., 1986. Precambrian continental crust of India and its evolution. The J. Geol. 94, 145–166. doi:10.1086/629020.
Vaidyanadhan, R., Ramakrishnan, M., 2010. In: Geology of India, 1. Geological Society of India, Bangalore, pp. 557–994.
Rao, V.V.S., Sreenivas, B., Balaram, V., Govil, P.K., Srinivasan, R., 1999. The nature of the Archean upper crust as revealed by the geochemistry of Proterozoic shales of the Kaladgi basin, Karnataka, Southern India. Precamb. Res. 98, 53–65. doi:10.1016/S0301-9268(99)00038-8.
Raha, P.K., Sastry, M.V.A., 1982. Stromatolites and Precambrian stratigraphy in India. Precamb. Res. 18 (4), 293–318. doi:10.1016/0301-9268(82)900067.
Roberts, N.M., 2013. The boring billion?–Lid tectonics, continental growth and environmental change associated with the Columbia supercontinent. Geosci.Front 4 (6), 681–691. doi:10.1016/j.gsf.2013.05.004.
Robinson, D., Warr, L.N., Bevins, R.E., 1990. The Illite crystallinty technique: a critical appraisal of its precision. J. Met. Geol. 8 (3), 333–344.

Saha, D., Bhowmik, S.K., Bose, S, Sajeev, K., 2016. Proterozoic tectonics and trans-Indian mobile belts: a status report. Proc. Ind. Nat. Sci. Acad. 82 (3), 445–460.
Shrivastava, J.P., Ahmad, M., 2005. Compositional studies on illite-smectite from iridium enriched and other infra(Lametas)/inter-trappean sediments from Deccan Traps. Indian J. Geochem. 20, 21–142.
Smykatz-Kloss, 1974. Differential Thermal Analysis. Applications and results in Mineralogy. Springer-Verlag, Berlin, pp. 81–87.
Thyne, G., 2001. A model for diagenetic mass transfer between adjacent sandstone and shale. Mar.Pet.Geol 18 (6), 743–755. doi:10.1016/j.marpetgeo.2015.01.006.
Velde, B., 1995. Origin and Mineralogy of clays: clays and the Environment. Springer-Verlag, Berlin, Heidelberg, p. 334.
Warr, L.N., Rice, H.N., 1994. Interlaboratory standardization and calibration of clay mineral crystallinity and crystallite size data. J. Met. Geol. 9, 141–152.
Weaver, C.E., 1989. In: Clays, muds and shales, Developments in sedimentology, 44. Elsevier, Amsterdam, p. 819.
Yang, C., Hesse, R., 1991. Clay minerals as indicators of diagenetic and Anchi-Metamorphic grade in an overthrust belt, External domain of southern Canadian Appalachian. Clay Miner. 26, 799–829. doi:10.1180/claymin.1991.026.2.06.
Yang, W., Zuo, R., Chen, D., Jiang, Z., Guo, L., Liu, Z., Chen, R., Zhang, Y., Zhang, Z., Song, Y., Luo, Q., 2019. Climate and tectonic-driven deposition of sandwiched continental shale units: new insights from petrology, geochemistry, and integrated provenance analyses (the western Sichuan subsiding Basin, Southwest China). Int. J. Coal Geol. 211, 103227. doi:10.1016/j.coal.2019.103227.
Young, G.M., 1988. Proterozoic plate tectonics, glaciations and iron-formations. Sediment. Geol. 58, 127–144.
Young, G.M., 2013. Precambrian supercontinents, glaciations, atmospheric oxygenation, metazoan evolution and an impact that may have changed the second half of Earth history. Geosci. Front. 4 (3), 247–261.
Zachariah, J.K., Bhaskar Rao, Y.J., Srinivasan, R., Gopalan, K., 1999. Pb, Sr and Nd isotope systematics of uranium mineralised stromatolitic dolomites from the proterozoic Cuddapah Supergroup, south India: constraints on age and provenance. Chem. Geol. 162 (1), 49–64. doi:10.1016/S0009-2541(99)00100-X.
Zhang, L., Sun, M., Wang, S., Yu, X., 1998. The composition of shales from the Ordos basin, China: effects of source weathering and diagenesis. Sediment. Geol. 116 (1-2), 129–141. doi:10.1016/S0037-0738(97)00074-2.